

Upper-mantle *S*-velocity structure of central and western South America

Suzan van der Lee¹, David James and Paul Silver

Department of Terrestrial Magnetism, Carnegie Institution of Washington, Washington DC 20015

Abstract. We have used broadband seismograms recorded at portable and permanent seismic stations in South America to image the three-dimensional *S*-velocity structure beneath central and western South America. We have interactively fitted the waveforms of *S* and surface wave trains in 500+ seismograms from 90 earthquakes and 60 different stations. The constraints on upper mantle *S*-velocity structure provided by the waveform fits have been combined with independent estimates of depth to the Mohorovičić discontinuity, yielding model SA99. The *S*-velocity structure of SA99 reveals a highly heterogeneous upper mantle with a maximum peak to peak *S*-velocity difference of 1 km/s above 100 km. The heterogeneity seems to be correlated with tectonic and geologic domains. SA99 shows high lithospheric *S*-velocities for the Precambrian cratons. The Amazon basin is also underlain by high *S*-velocities while three other intra-platform basins are underlain by low *S*-velocities at various depths. SA99 shows extremely low *S*-velocities in the mantle wedge beneath the volcanically active Andes. We explain these low *S*-velocities as originating from realistic amounts of volatiles, released by the subducting Nazca crust, and resulting amounts of partial melt within the peridotitic mantle wedge, without requiring elevated temperatures. While SA99 could be consistent with diffuse influx for corner flow in the mantle wedge, it does not support models that require influx of subcontinental upper mantle into the mantle wedge through a laterally uniform low-viscosity channel.

1. Introduction

South America is an assembly of all classified types of tectonic environments, from Precambrian shield, through flood basalt province and sedimentary basin, to mountain range (Figure 1). The South American Precambrian shields are found in Brazil, Venezuela, Guyana, Surinam and French Guiana, with edges in Bolivia and Colombia. The shield regions are composed of Archaean nuclei, such as the São Francisco craton, and Proterozoic mobile belts [Cordani and Brito Neves, 1982]. The Amazon basin is an elongated basin composed of the Solimões basin in the west and the Amazonas basin in the east, with 4 to 6 km, respectively, of sediments along the central axis [Milani and Zalán, 1999]. The Amazon basin is thought to be related to a failed rift system [Satzmari, 1983]. The Chaco, Pantanal and Paraná basins are much less elongated, with aspect ratios closer to 1. The Paraná basin is a province of 140–120 Ma old flood basalts covering the basement together with up to 5 km pre- and post-volcanism sediments [Piccirillo and Melfi, 1988; Milani and Zalán, 1999]. The Pantanal wetland basin is filled with up to 0.5 km sediments [Ussami *et al.*, 1999] while the much larger Chaco basin is filled with up to 4 km sediments [Horton and DeCelles, 1997] derived from erosion of the adjacent and parallel Andes mountain range. The Andes mountains are folded and thrust crust, are seismically and magmatically active, and contain rich mineral resources. The Andes between 4°S and 47°S were formed due to subduction

of the Nazca plate under the South American plate [James, 1971b; Gansser, 1973; Ramos, 1999]. Nazca subduction occurs at an angle near 30° in the central section of the Central Andes between 14°S and 24°S, while flat subduction takes place north and south of there, between 6°S and 14°S and between 24°S and 32°S, respectively [Cahill and Isacks, 1992; Ramos, 1999]. Dip angles of the subducting Nazca plate have also changed through geologic time [James and Sacks, 1999].

In this study we investigate whether and to what extent the different tectonic and geological terranes of South America are reflected in the structure of the upper mantle beneath the continent. If the South American tectonic plate extends to considerable depth in the upper mantle or if mantle flow under the plate is coherent with the plate's motion, we may expect South America to overly a highly heterogeneous upper mantle, in accordance with its tectonic and geological diversity. If, however, South American plate motion is decoupled from deeper upper mantle motion we expect to find a low-viscosity layer in the upper mantle, showing little correlation with surface tectonics and geology. Moreover, we would expect this layer to partake in corner flow in the mantle wedge over the subducting Nazca plate beneath the Andes.

Upper mantle structure of South America has been imaged in global scale tomographic studies but these do not show structure at the geological scales of Figure 1 either due to their very large resolution lengths [$> 10^3$ km, e.g. Li and Romanowicz, 1996; Ekström and Dziewonski, 1998] or due to lack of resolution for the uppermost mantle away from the Wadati-Benioff zone [e.g. Bijwaard *et al.*, 1998]. Regional phase and group velocity maps contain information about upper mantle structure on shorter ($< 10^3$ km) resolution length scales. The group velocity maps of Vdovin *et al.* [1999] begin to show considerable heterogeneity for the seismic velocity structure of South America. Vdovin *et al.* [1999] interpret the mapped heterogeneities in group velocity as being caused by the presence of sediments in the Chaco and Paraná basins, thicker crust

¹ now at: Institute of Geophysics, Eidgenössische Technische Hochschule, Zürich, Switzerland

Copyright 2001 by the American Geophysical Union.

Paper number 2001JB000338.
0148-0227/02/2001JB000338\$9.00

under the Andes, and cratonic keels in the upper mantle under the Guyana and Brazilian shields. The mapped group velocities do not, however, relate unambiguously to crust and upper mantle structure at particular depths. The western hemisphere S -velocity model of *Grand* [1994] includes the upper mantle of northern South America, where high S -velocity Precambrian cratons predominate. A regional phase velocity study by *Snoke and James* [1997] inferred very low S -velocities beneath the Chaco basin but it provides little information on the lateral extent of this low velocity region. Higher resolution regional studies tend to focus on a specific region within South America and/or resolve a limited depth range of upper mantle structure. *Engdahl et al.* [1995] and *VanDecar et al.* [1995b] have resolved the high-velocity structure of the subducting Nazca plate in the mantle beneath the central Andes from P -wave travel times. However, due to their event-station distribution they do not resolve uppermost mantle structure away from the subducting plate. *VanDecar et al.* [1995a] and *Schimmel et al.* [2001] have resolved a deep low velocity fossil plume beneath the eastern Paraná basin but their model does not extend beyond the margins of the BLSP [*James et al.*, 1993] seismic networks. On a smaller scale, *Myers et al.* [1998] have used local body wave travel times to image P and S -velocity structure in the mantle wedge beneath southwestern Bolivia.

The growing number of permanent and portable broad band seismic stations in South America, together with the development of sophisticated waveform analysis techniques, has created an opportunity to circumvent the limitations in lateral resolution, depth resolution and geographical coverage of global and regional studies discussed above. The deployments of portable seismic networks in central South America enables unprecedented resolution of seismic structure across the width of the continent. In this study we derive a 3-D S -velocity model for the South American crust and upper mantle by modeling wave trains containing S - and surface wave arrivals recorded at permanent and portable South American stations. The distribution and characteristics of events and recording stations in our study yields a resolution that strongly varies spatially but is

several hundred km in the well resolved regions. While our event-station distribution is not capable of resolving 3-D S -velocity structure for northeastern and southern South America, 3-D S -velocity structure is well resolved for central and western South America.

2. Method

We used the method of Partitioned Waveform Inversion (PWI) [*Nolet*, 1990] in the form described by *Van der Lee and Nolet* [1997]. Originally, *Nolet* [1990] applied the method in two dimensions to data from the linear NARS array [*Dost et al.*, 1984]. PWI was first applied to retrieve three-dimensional (3-D) upper mantle structure by *Zielhuis and Nolet* [1994]. Here, we apply PWI to image the 3-D S -velocity structure of the upper mantle of western and central South America using vertical component seismograms recorded by South American stations. These seismograms are from a mix of relatively uniformly distributed, permanent stations and from concentrated groups of stations from temporary experiments using portable seismometers [*Van der Lee et al.*, 2000], as described in the next section. This combination results in a wave path coverage and resulting spatial resolution that is less uniform than in some other 3-D applications of PWI [*Van der Lee and Nolet*, 1997; *Simons et al.*, 1999; *Lebedev and Nolet*, 2001]

Van der Lee and Nolet [1997] introduced an inversion for S -velocity parameters defined at nodes of a 3-D Cartesian grid to prevent biases introduced by cell size variation with latitude and depth that is unrelated to the sensitivity of the data to the model parameters. Biases introduced by non-uniform wave path coverage, such as the South American coverage, are expressed in relatively bad resolution in regions of sparse wave path coverage, such as the seismically inactive margins of the continent, and relatively good resolution in regions of dense wave path coverage, such as near the locations of the temporary seismic experiments in South America. For presentation purposes, for computational efficiency, or for integrated quantitative interpretation such geographical biases could be elegantly incorporated by using a variable grid spacing [*Sambridge and Gudmundsson*, 1998; *Bijwaard et al.*, 1998], where smaller cells are used for regions of denser ray coverage. However, in our present application to South America, our interests are restricted to the S -velocity structure in the regions of dense wave path coverage, e.g. the target regions of seismic experiments. Our data set from the mix of portable and permanent stations in South America provides non-uniform resolution. The resolution is dominated by damping and smoothing in regions of sparse wave path coverage and the resolution is good throughout the uppermost mantle in central and western South America, as discussed in detail in a following section.

In applying PWI, we have extracted linear constraints on average earth structure between an earthquake and a station by non-linear waveform fitting of wave trains composed of fundamental and higher mode surface waves. Due to severe ambiguities in the interpretation of Rayleigh wave amplitude anomalies [*Van der Lee*, 1998] we do not include the amplitude differences between observed and synthetic wave trains explicitly as constraints on earth structure. Hence the waveform fits are dominated by phase matches for the waves of various modes and frequencies in the fitted wave train. We use different 1-D starting models for different seismograms, depending on the character of the path followed by the waves. For continental wave paths we use the *iasp91* model [*Kennett and Engdahl*, 1991] with densities from the PEM-C model [*Dziewonski et al.*, 1975]. For the quality factor for shear waves, Q_s , we follow *Snoke and James* [1997] and use a constant value of 200 throughout the upper mantle, as a reasonable average of the complex variations in Q_s beneath South America [*Sacks and Okada*, 1974]. For paths

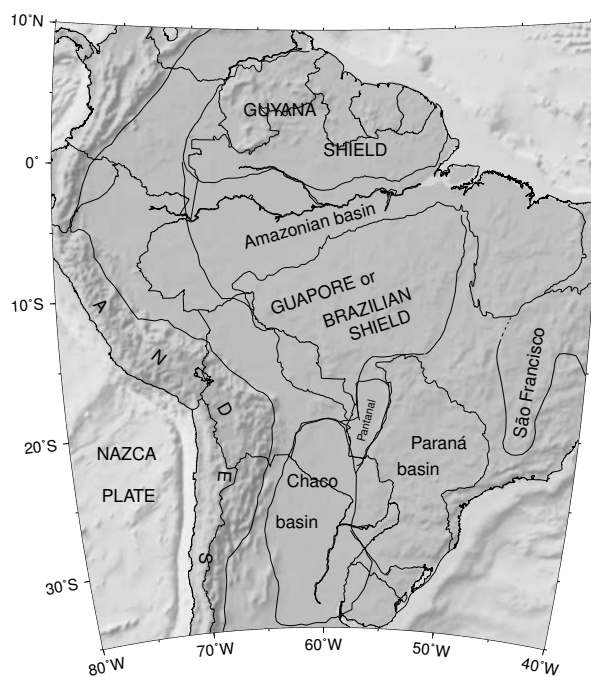


Figure 1. Geologically labeled map of the part of South America studied here. Background topography and bathymetry are shaded.

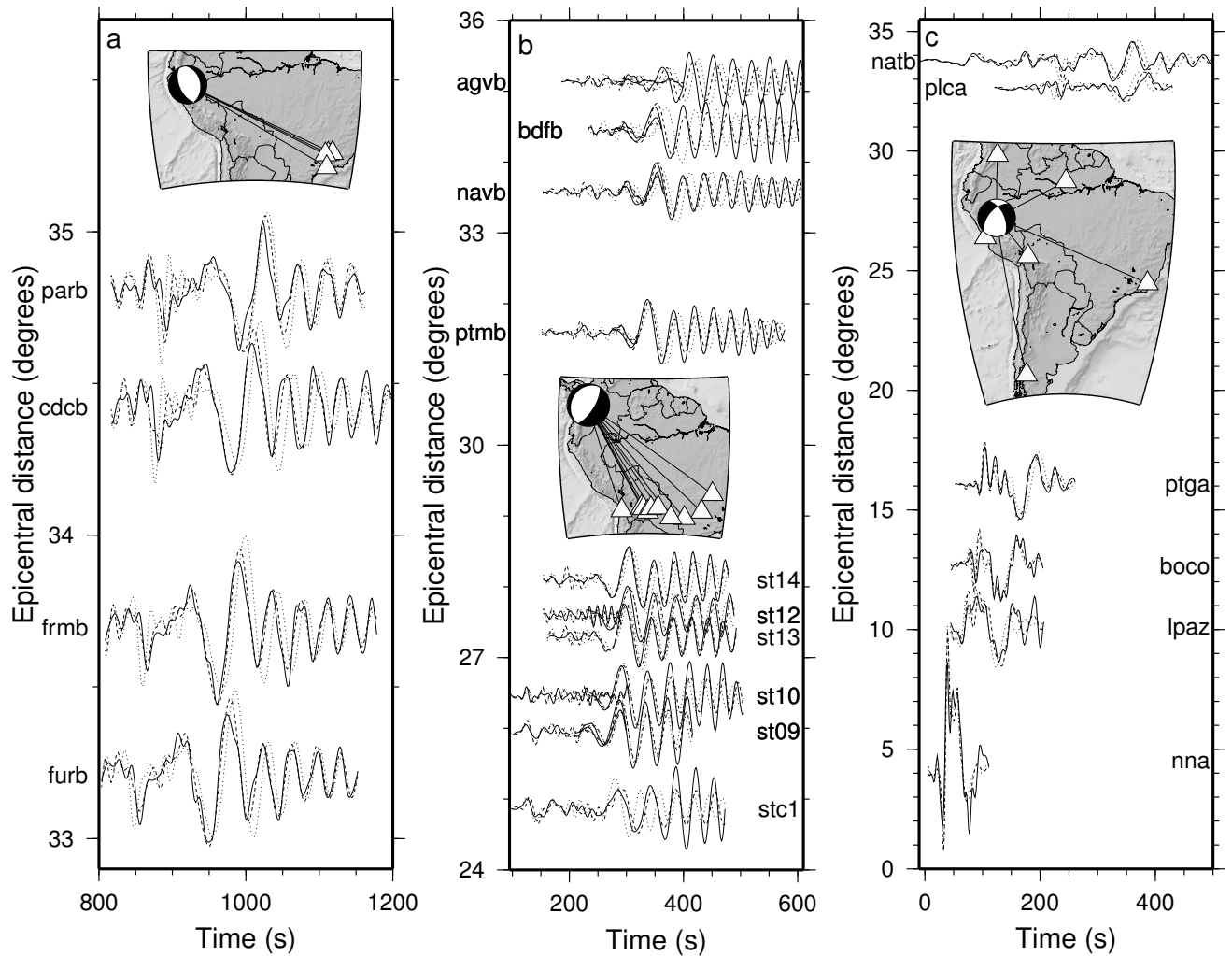


Figure 2. (a) Observed seismograms (solid lines) and synthetic seismograms for *iasp91* (dotted lines) and a posteriori synthetic seismograms for 3-D model SA99 (dashed lines) for the event on January 20, 1994, mb 5.6 in Peru. “Final” fits to individual seismograms from an intermediate stage of PWI are not shown. Insets show maps with the focal mechanism of the event, the wave paths, and the stations. Topography is shaded. (b) Same as Figure 2a but for February 8, 1995, mb 6.2 Colombia. A reduction velocity of 6 km/s was used. (c) Same as Figure 2a but for April 24, 1996, mb 5.6 Peru. A reduction velocity of 6 km/s was used.

traversing the Nazca plate or the Atlantic Ocean we use a starting model similar to *iasp91*, but with a crustal structure typical for oceanic crust [Nishimura and Forsyth, 1989], with a total thickness of 6 km below a 4 km deep ocean. For paths crossing comparable amounts of both ocean (Pacific/Atlantic) and continent we again use a model similar to *iasp91*, but with a water layer and a 25 km thick crust, reflecting the mixed character of the path. The fits to South American waveforms from continental propagation indicate that the continental crust is on average somewhat thicker than the 35 km of *iasp91*. Consequently, we use *iasp91* with crustal thickness modified to 40 km as the reference model in the inversion for the 3-D model.

We invert simultaneously for S -velocity and for depth to the Mohorovičić discontinuity (Moho), following Das and Nolet [1995] and Gomberg et al. [1988]. In our study, Rayleigh waves alone cannot uniquely determine Moho depth together with the S -velocity structure of uppermost mantle and crust. We therefore include additional, independent constraints on Moho depth in the inversion to allow for a better separation of the effects of S -velocity and crustal thickness on the Rayleigh wave trains. We use results from re-

ceiver function analysis [Beck et al., 1996, Assumpção et al., 2002] as firm independent constraints on Moho depth beneath the Bolivian and Brazilian stations. We assume that the crust is in isostatic equilibrium where the constraints from receiver function analysis or from the Rayleigh waveform fits do not require otherwise. To compute the Moho depths predicted from isostasy we use average densities at the surface of $2.7g/cm^3$, $2.9g/cm^3$ for the lower crust and $3.3g/cm^3$ for the underlying mantle. The results of these predictions are similar to results based on extrapolated crustal types used for South America in model CRUST5.1 [Mooney et al., 1998].

We have jointly inverted the constraints from waveform fitting and receiver function analysis, for S -velocity and for crustal thickness. Further following Van der Lee and Nolet [1997], the S -velocity is parameterized as coefficients for nodes of a Cartesian grid, while the crustal thickness is parameterized as nodes of a triangular tessellation on a sphere. The distance between the Cartesian nodes in the z -direction is 50 km. This distance in the x - and y -direction as well as the distance between the triangular nodes is roughly 90 km. We search for the best fitting smooth model, using a smoothing radius of 180 km in the longitude-latitude plane. Using a larger smoothing

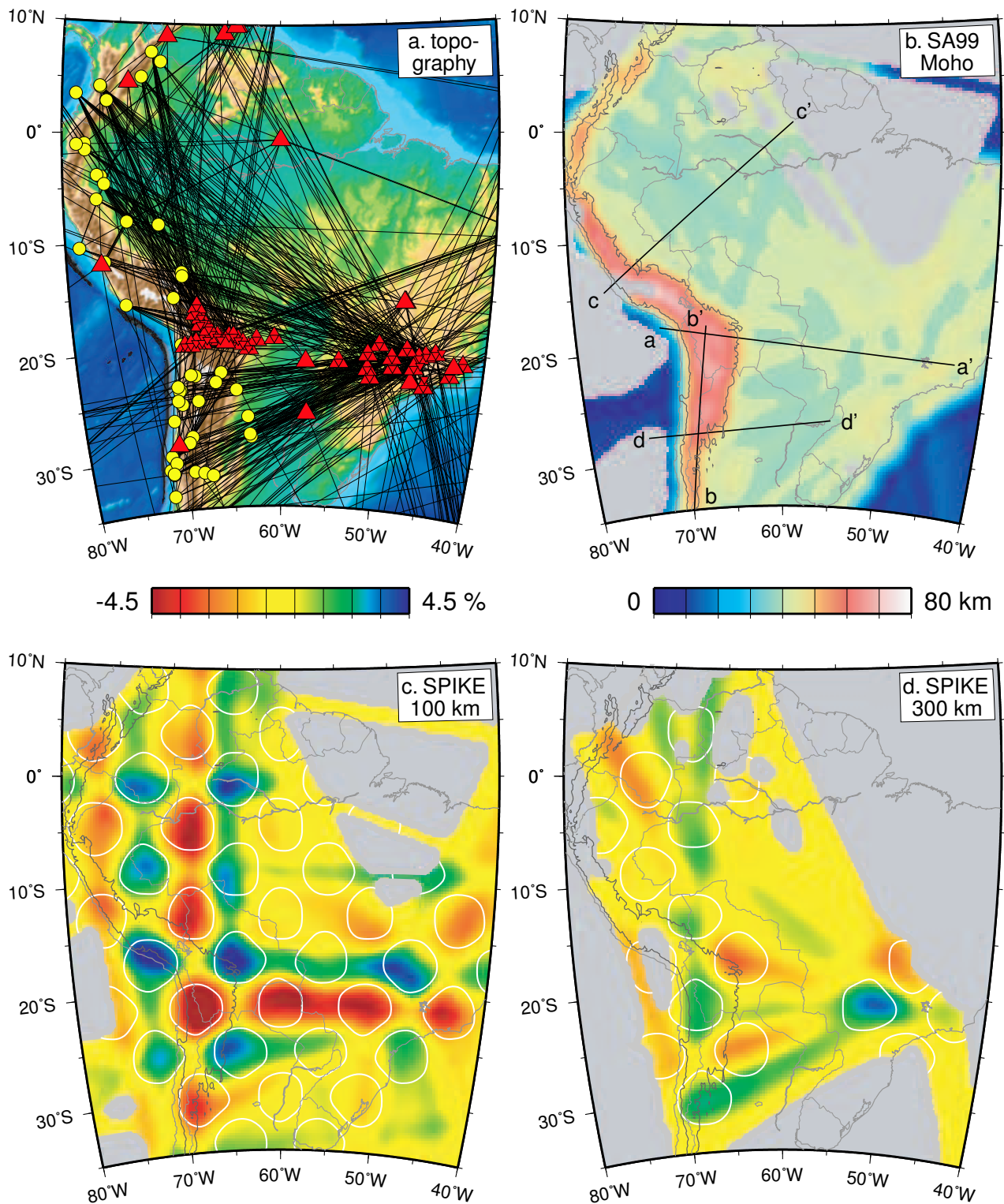


Plate 1. (a) Topographic map of South America with the events (yellow circles), stations (red triangles), wave paths (black lines), and receiver function locations (small inverted red triangles) used in the inversion for SA99. (b) Depth to the Mohorovičić (Moho) discontinuity in SA99. The cross sections shown in Plate 3 are taken along the black great circle segments shown on this map. The darker grey contour represents the 2 km elevation contour. (c) Spike resolution test results at 100 km. The input model is represented by the white contours at $\pm 3.5\%$. (d) As c but at a depth of 300 km and with fewer spikes.

radius does not lead to a significantly different model. Using a larger node spacing for the grids leads to a model with sharper velocity gradients. The inversion problem is mixed determined and is solved

using the damped least-squares inversion method as implemented by Van der Lee and Nolet [1997], with damping parameter $\lambda = 1$. The inversion converged to a remaining root-mean-square (RMS)

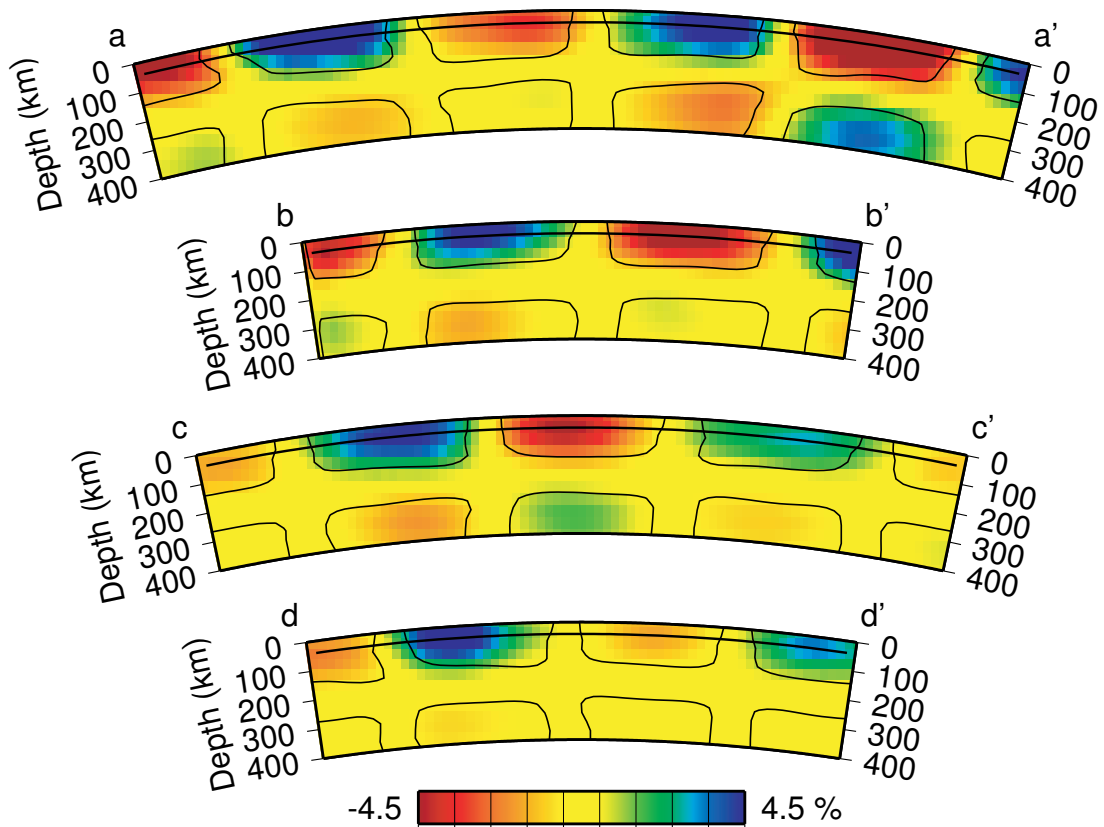


Figure 3. The same four vertical cross sections as in Plate 3, but showing the results of a series of spike resolution tests. The -3.5% and $+3.5\%$ levels of the anomalies in the input model are indicated by the thin black contours. The anomalies of the output model are shaded with the shown color scale.

residual for each waveform constraint corresponding to 14% of the initial waveform misfits. The initial overall RMS waveform misfit was reduced by 58%.

3. Data

The coverage of South America with permanent broadband stations has improved significantly in the last decade from 1 station in 1993 to 9 installed stations in 1996. Moreover, in the same period an impressive amount of broadband data has been collected from limited-duration seismic experiments with portable seismometers. We selected vertical component seismograms of events from the period 1992 through 1996 that are recorded by one or more stations from the seismic experiments BLSP92 [James *et al.*, 1993], BANJO/SEDA [Beck *et al.*, 1994], BLSP95 [Assumpção *et al.*, 2002], or VEN92 [Russo *et al.*, 1996] with a good signal to noise ratio for *SV* and/or Rayleigh waves. In addition we collected seismograms of these events from the IRIS-DMC that were recorded by permanent stations of the Global Seismic Network in and around South America. In particular, these seismograms were recorded by the GTSN, IRIS/IDA, and IRIS/USGS networks. Our data selection and subsequent analysis yielded fitted waveforms of 554 vertical component seismograms from 90 events and 60 different stations. Of these 554 seismograms 87 were recorded by permanent stations and 467 by the portable experiments (276 by BLSP92, 109 by BANJO, 41 by BLSP95, 11 by VEN92, 19 by SEDA, and 11 by the Carnegie station LCOC). The relatively short period SEDA seismograms could be fitted by using the results from fitted BANJO seismograms as starting models. The selected events are both regional and teleseismic, shallow and deep, and they range in magnitude from 4.6 to 6.6. For the generation of synthetic seismograms for these events we assume the ISC hypocenter and origin time as well

as the Harvard CMT solution, along with an earth model that approximates average earth structure near the source. Only azimuths away from the fundamental-mode Rayleigh-wave source-radiation nodes have been considered. Our diverse set of events together with our heterogeneous collection of portable and permanent stations precludes any automated waveform fitting process. Instead, each seismogram was subjected to interactive quality control [Van der Lee, 1996], and its waveforms were fitted interactively as well. Plate 1a illustrates the distribution of events, stations, great circle wave propagation paths, and receiver function models.

A total of 3362 significant linear constraints were derived from the waveform fits and have been inverted for *S*-velocity structure together with the independent estimates of crustal thickness. Solving the inverse problem yielded our 3-D *S*-velocity model SA99. We used SA99 to compute *a posteriori* waveform misfits [Van der Lee and Nolet, 1997]. As expected, the *a posteriori* misfits show a much narrower distribution than the *initial* misfits for the 1-D reference model. Also as expected, the *a posteriori* misfit distribution is slightly wider than that for the *final* misfits, which are based on the best-fitting 1-D models for individual seismograms. Figure 2 shows some of the seismograms that have been used in the inversion. The seismograms are shown with *initial* and *a posteriori* synthetic seismograms, based on *iasp91* and SA99, respectively. The latter synthetic seismograms fit the observed seismograms from both temporary and permanent stations well. Figure 2 also shows that both the fundamental mode Rayleigh wave trains and the higher-mode/body-wave trains are fit well by SA99.

4. Resolution

The wave path coverage of Plate 1a suggests that the best resolution for our model SA99 is expected for central and western South America, where the density and azimuthal coverage of the wave

paths is best. Most of the events used are located in the Wadati-Benioff zone, while the stations recording the events are on the continental side of the zone. Therefore, the wave trains used in this study are relatively sensitive to mantle structure on the continental side of the Wadati-Benioff zone while they are less sensitive to the velocity structure of the subducting Nazca plate, the largest part of which underlies the Wadati-Benioff zone [Engdahl *et al.*, 1997]. To assess the spatially varying resolving power of our data in more detail we have carried out a large variety of standard resolution tests.

For each test synthetic data with added random noise are inverted using the data sensitivity matrix computed from the observed data. The tested structures range from unrealistic but traditionally tested patterns of spikes of alternating amplitude, via more realistic models (hypothesizing anomalies representing subducting lithosphere, hydrated mantle wedge, and cratonic lithosphere, for example) to a uniform upper mantle anomaly. In this paper, we can only show a subset of the performed resolution tests. In summary, and not surprisingly, our resolution tests show that 1) spatially bigger anomalies are better resolved than smaller anomalies, 2) the damping applied reduces the absolute values of the recovered anomalies, especially in regions of lower combined sensitivity, 3) in regions where the wave paths fall within a narrow azimuth range, imaged anomalies represent the laterally averaged anomaly along the wave paths, which becomes more apparent with depth, where sensitivity is lower, and 4) vertical smearing is negligible, owing to the combined sensitivity of body- and surface-waveforms.

The results of our spike resolution tests, shown in Plates 1c, 1d and Figure 3, illustrate most of these features. The input model for these resolution tests contains limited-size S -velocity anomalies of alternating sign. The input spike models have extrema of $\pm 6.5\%$ relative to *iasp91*. The resolution of these relatively narrow spikes presents a lower limit for the resolution of upper mantle structure related to the larger tectonic domains of the South American continent. For the largest part of South America the resolution of SA99 below 400 km is not useful. Above 400 km there are strong variations in resolution, laterally and with depth. Plate 1c and d show that, as expected, some of the recovered spike anomalies are laterally smeared. Spike resolution at a depth of 300 km is fair for the central Andes and is best in the eastern part of the model. At a depth of 100 km the spike resolution is best for central and western South America.

The cross sections through our model SA99 in Plate 3 are accompanied by the input and recovered anomalies of one of our resolution tests with hypothesized structures that might be considered as realistic. The input model contains a dipping $+9\%$ anomaly, representing subducting lithosphere, an adjacent, parallel dipping -6.5% anomaly, representing a mantle wedge on which depth resolution can be tested, as well as a horizontal -6.5% layer, representing a possible subcontinental low-velocity layer. Plate 3 shows that, as expected, resolution for the anomaly representing subducting lithosphere is not nearly as good as resolution for the continental anomalies. However, at particular depths and in particular parts of the region covered by our data this subducting-plate anomaly is resolved. For the anomalies representing the mantle wedge and the subcontinental low-velocity layer the resolution for recovery of the strength of the anomaly is heterogeneous. The resolution below 300 km varies laterally from none to good. However, above 300 km the spatial resolution for these anomalies is very good. Plate 3 and Figure 3 show that, as expected, the anomalies do not smear vertically. In the next sections we discuss model SA99, only for the best-resolved regions.

5. Results

Model SA99 consists of the 3-D South American upper mantle S -velocity distribution and Moho depth. The latter is shown in Plate 1b. This Moho map shows the Andes having a very thick (up to 70

km) crust, which is consistent with results from an early surface wave analysis by James [1971a]. The S -velocities of SA99, relative to the S -velocities of *iasp91*, are shown in Plate 2 for different depths in the upper mantle. Discussion and interpretation of the features of SA99 that are well resolved is deferred to the next section. Here we first present and describe the major anomalies of the well resolved regions of SA99: 1. Most of the part of Brazil that is covered by our data as well as southern Venezuela and eastern Colombia are underlain by high S -velocities (see 100 km map), locally up to 4.7 km/s. In the next section we interpret these anomalies as representing Precambrian cratonic lithosphere. 2. Low S -velocities have been imaged beneath the Pantanal basin (central anomaly on the 200 km map) as well as beneath the Chaco basin and the western Paraná basin (anomalies in northern Argentina and east of Paraguay, respectively, on the 100 and 150 km maps). The lateral extent of these anomalies is better resolved in the north-south direction than in the west-east direction, as can be inferred from the spike resolution test in Plate 1c. S -velocities around 4.3 km/s are located beneath the eastern Paraná province (the easternmost low-velocity anomaly on the 300 km map). 3. Although the region through which the Amazon river flows is also a basin, it is not underlain by low velocities but by high velocities similar to those imaged for the Precambrian cratons. 4. SA99 shows extremely low S -velocities of 4 km/s in the mantle wedge around 100 km beneath the highest topography of the Andes. The imaged low velocity anomalies lie just east of the contours outlining the Wadati-Benioff zone [Hasegawa and Sacks, 1981; Cahill and Isacks, 1992], confirming their interpretation (next section) as slab-overlying mantle wedge material. 5. Relatively high velocities have been imaged parallel to the Andes at depths around 150-200 km. The imaged high velocity anomalies lie just west of the slab contours confirming their interpretation as subducting Nazca lithosphere. These high velocities do not form a continuous unit, mainly due to strong variations in resolution for the subducting lithosphere below the Wadati-Benioff zone (Plate 3). We document these features in more detail by showing four vertical cross sections through SA99 in the 2nd and 3rd frames of Plate 3a through d.

The cross section in Plate 3a runs through the region with densest station coverage, dominated by the BLSP and BANJO networks (1st frame). The bottom two frames of Plate 3a show the input and output models of a resolution test. The test shows that the resolving power is very good for a hypothesized layer of anomalous velocity (whether low or high) between 150 and 250 km. However, such an anomaly is not imaged at these depths in SA99 (2nd and central frames). For this cross section, the dipping high and low velocity anomalies in the western part (bottom frame) cannot be resolved (4th frame) below some 250 km. Above the Wadati-Benioff zone of relocated hypocenters [Engdahl *et al.*, 1998] SA99 (central frame) shows the extremely low velocity (4 km/s) mantle wedge directly beneath the crust of the Altiplano and eastern Cordillera of the Andes. Another low velocity (-4%) anomaly has been imaged in the center of the profile. This anomaly underlies the northern Chaco and the Pantanal basins and it extends from beneath the crust to roughly 350 km. At near-transition-zone depths we have imaged a low velocity (4.3 km/s) anomaly beneath the eastern Paraná basin and southern São Francisco craton, on the east side of the profile. This cylindrical anomaly extends from a depth of 100 km down into the transition zone. The western Paraná basin, slightly south of profile aa', is underlain by low velocities at a much shallower (100 km) level. The eastern part of the profile also shows the relatively high-velocity lithosphere of the São Francisco craton.

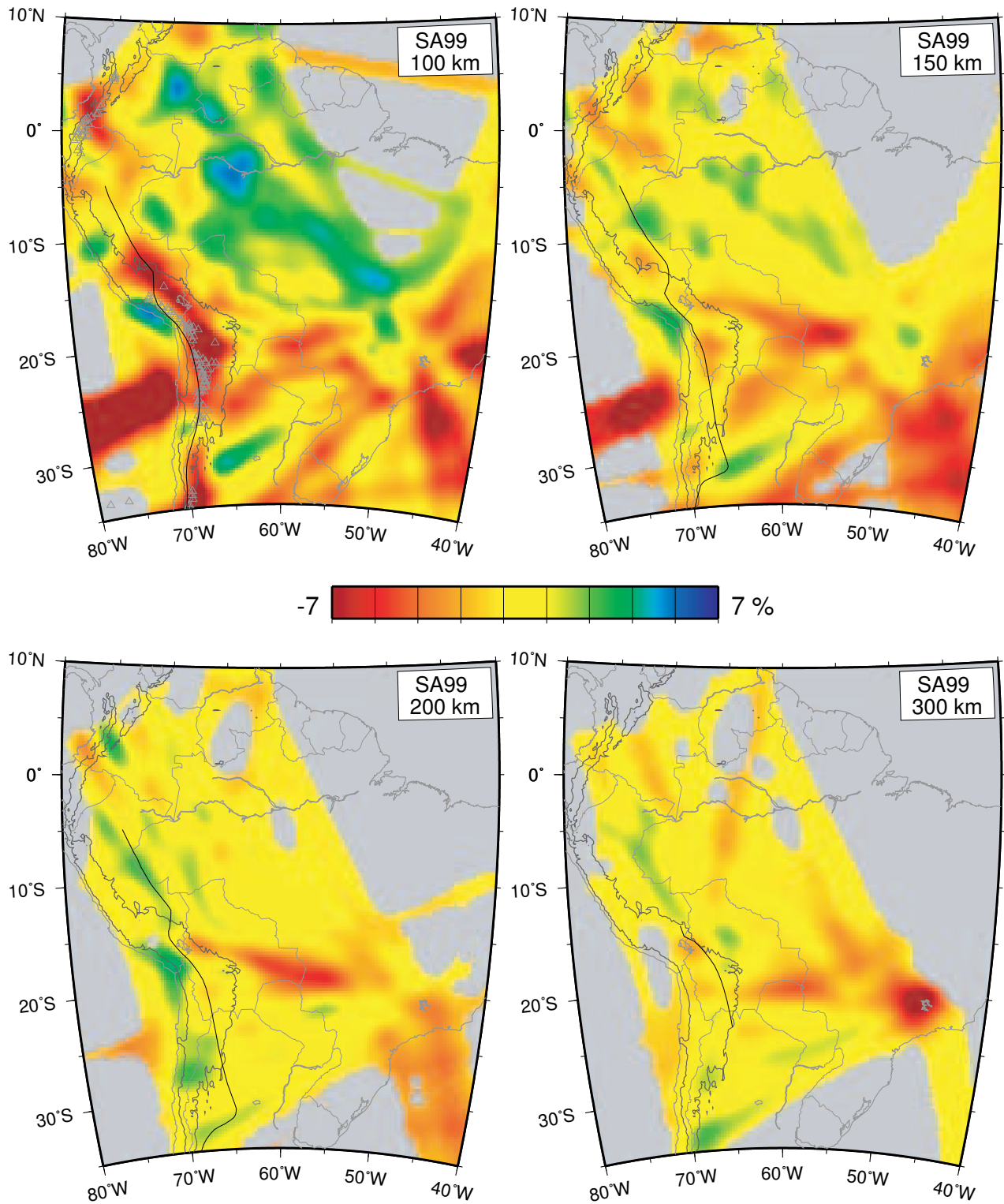


Plate 2. SA99 at depths of 100 150 200, and 300 km. The 2-km elevation and seismicity [Hasegawa and Sacks, 1981; Cahill and Isacks, 1992] are contoured with fat grey and black lines, respectively. Historical and active volcanoes are represented by light grey triangles [James and Sacks, 2000]. Areas to which our data have negligible sensitivity are made grey. The color scale is saturated. Resolution varies laterally (see Plates 1 and 3, and Figure 3).

Plate 3b shows a cross section along the strike of the Andes and the underlying extremely low velocity mantle wedge. The resolution test in the bottom two frames shows that the low velocity anomaly in the mantle wedge is spatially well resolved, though somewhat damped to a less extreme value. This test also shows

that, as expected, the anomaly representing subducting lithosphere is strongly damped and locally unresolved. Plate 3b shows that the mantle wedge of SA99 (2nd and central frames) dips from the center of the profile (at 26.5°S) gently to the north. This dip is in accordance with the variation in dip of the subducting Nazca plate

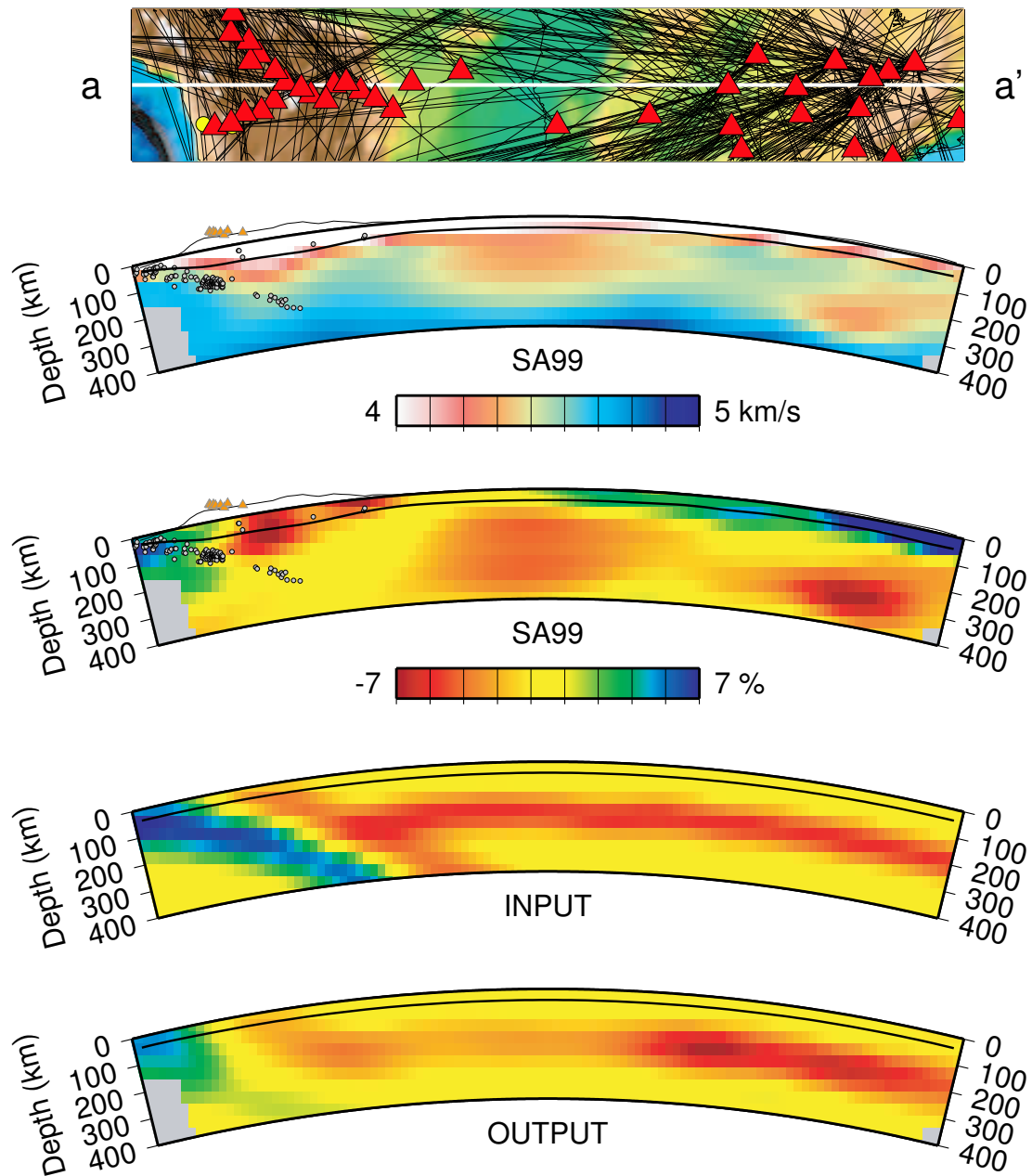


Plate 3a. Vertical cross section aa' through SA99 and a resolution test, taken along great circle segments. First panel is a map astride the great circle segment, keyed to the segments mapped in Plate 1b; second panel is a cross section through the absolute S -velocity of SA99; third panel is a cross section through the SA99 anomalous S -velocity relative to *iasp91* (the color scale is saturated); fourth panel is a cross section through the input model of the resolution test with a hypothetical mantle structure (which is not designed to imitate SA99, but simply represents one possible concept of realistic mantle structure); and fifth panel is a cross section through the results of this resolution test (resolution does not depend on the sign of the anomaly). The thick black lines represent the Moho. In the second and third panels the thin black line and the grey-lined small orange triangles represent 10 times exaggerated topography and volcanoes, respectively. The grey dots are hypocenters [Engdahl *et al.*, 1998] within 1° of the profile.

along the strike of the Andes [Cahill and Isacks, 1992]. The cross section shows a good correlation between the well resolved bottom of the low-velocity mantle wedge and the superimposed earthquake hypocenters from the independent data set of Engdahl *et al.* [1998]. The imaged high velocity anomalies beneath the low velocity mantle wedge (3rd frame of Plate 3b) are likely related to subducting Nazca lithosphere.

Plate 3c shows a cross section through the Peruvian Andes and the western Amazon basin. The north-eastern half of this cross sec-

tion through SA99 shows the high velocity anomaly beneath the western Amazon basin extending down to roughly 150 km, below which our data still have resolving power (Figure 3). The bottom two frames of Plate 3c show that a (high or low) velocity anomaly at 200 km would be resolved by our data, though damped to a lower extreme value. Flat subduction is on-going on the south-western side of this profile [Cahill and Isacks, 1992], as indicated by the hypocenters in the 2nd and 3rd frames for SA99. Low velocities are confined to the region above the Wadati-Benioff zone. Although our data cannot resolve high velocity slab material directly below the

flat Wadati-Benioff zone for this profile, our data do have resolving power for deeper levels, including for the high velocity anomaly at 300 km just northeast of the Andes (see also Figure 3c).

Plate 3d shows a cross section through the Andes in central Chile where the dip angle of subduction is decreasing from north to south [Cahill and Isacks, 1992]. The bottom two frames show that the subduction-related high-velocity anomaly imaged in SA99 (central frame) is resolved down to 250 km. The lateral extent of this high-velocity anomaly of SA99 is consistent with the relatively shallow dip of the Wadati-Benioff zone. A low *S*-velocity anomaly is visible beneath the central Chaco basin near the center of this profile, despite the somewhat weaker resolving power for this region. The eastern part of this profile shows a high-velocity anomaly likely related to the lithosphere of northern Argentina.

6. Discussion

6.1. Correlation with continental surface

The results presented in the previous section show that there is a strong correlation between the imaged heterogeneity in South American upper mantle *S*-velocity structure (Plates 2 and 3) and the tectonics and geology of the continent (Figure 1). Model SA99 shows no evidence for a uniform subcontinental low velocity layer as hypothesized in the resolution test shown along with SA99 in Plate 3. The frames of Figure 3 showing absolute *S*-velocity of SA99 indicate that velocity minima are found along the profiles at depths varying from subcrustal to 250 km (excluding the deep easternmost anomaly in profile aa'). However, this minimum-velocity track along the profiles show little continuity with the low-velocity mantle wedge. Therefore it is unlikely that large amounts of mantle flow are concentrated in this low-velocity track. Its possible role as a low-viscosity layer that decouples plate motion from upper-mantle flow is thus highly questionable. The correlation between *S*-velocity structure and surface tectonics and geology is more consistent with previous work [VanDecar et al., 1995a; Russo and Silver, 1996; Meijer and Wortel, 1992; Silver et al., 1998] showing that South-American upper-mantle motion is coherent with plate motion. In this section we discuss the resolved *S*-velocity heterogeneity of SA99 in detail.

6.2. Precambrian cratons and intra-platform basins

The low *S*-velocity anomaly beneath the Chaco basin confirms the conclusion of the 2-D surface wave analysis by Snoke and James [1997]. This low-velocity anomaly beneath the Chaco and the more deeply extending low *S*-velocity anomaly beneath the Pantanal basins (Plate 3a) may indicate the presence of hotter mantle material than implied by the *iasp91* model. A temperature rise of some 200°C would explain the -4% *S*-velocity anomaly [Goes et al., 2000]. The deep cylindrical low-velocity anomaly beneath southeastern Brazil can be interpreted as the *S*-velocity image of the fossil plume proposed by VanDecar et al. [1995a]. Similar features have been imaged by Kennett and Widiyantoro [1999] beneath the Decan Traps and by Richardson et al. [2000] beneath the Ontong-Java plateau.

The high velocity anomalies (Plate 2) at 100 km depth in Brazil, southern Venezuela and eastern Colombia can be related to cratonic lithosphere of the various Archaean and Proterozoic terranes that compose the South American Precambrian shields. In particular, the lithosphere beneath the western Guaporé shield, the western Guyana shield, and the western Amazon basin extends to depths of roughly 150 km. High velocity lithosphere has consistently been imaged beneath world-wide Precambrian shields and its appearance beneath the South American shields is expected [e.g. Jordan, 1988]. The depth extent and velocity anomaly of the cratonic lithospheric

in SA99 are not as large as for the lithosphere of the North American craton in 3-D *S*-velocity model NA95 [Van der Lee and Nolet, 1997]. Model NA95 is better resolved in shield areas than SA99. However, if the South American craton is equally anomalous and extends equally deep as the North American craton our data would yield a stronger and deeper-reaching velocity anomaly for the westernmost part of the craton than that present in SA99. This indicates that the South American craton is likely to be weaker and/or thinner than the North American craton, which is in agreement with an observed difference in thickness of more than 50 km between these cratons [Grand, 1994]. However, our data cannot resolve the large eastern parts of the upper mantle beneath the Precambrian shields of South America, which leaves the average thickness and strength of all of the South American cratonic lithosphere unknown.

Among the sedimentary strata of the Amazon basin is evidence for Mesozoic magmatism, and it has been suggested that subsidence of the basin was initiated by rifting [Milani and Zalán, 1999]. Considering this significant post-Precambrian tectonic activity, it is surprising that the Amazon basin is underlain by thick, high *S*-velocity lithosphere. From the presence of these well-resolved (Plate 1c, 3c and Figure 3) high lithospheric velocities we infer that the Amazon basin is still part of the Amazonian craton, which comprises the Guyana shield to the north and the Guaporé shield to the south of the basin [Gibbs and Wirth, 1986]. Several geochronological provinces of the Amazonian craton can be traced from one of these two shields to the other on the opposite side of the basin [Tassinari and Macambira, 1999]. The inference that the Amazon basin is underlain by high-velocity lithosphere of the Amazonian craton implies that the upper-mantle part of the Amazonian craton is still largely intact and was not severely affected by the Mesozoic formation of the Amazon basin across the craton. The unexpected combination of high velocity Precambrian lithosphere underlying a Mesozoic basin could further imply that this Precambrian lithosphere has a different composition, causing it to be less buoyant than cratonic lithosphere underlying Precambrian shields or that its buoyancy is compensated by a thinner crust. SA99 seems to support a slightly thinner crust but this result is not well constrained.

The high *S*-velocity lithosphere in SA99 of the southern São Francisco craton in eastern Brazil (Plate 3a) extends to depths slightly less than 100 km if the bottom of the lithosphere is defined as the bottom of the region that has higher velocities than *iasp91*, and extends to depths near 150 km if the bottom of the lithosphere is defined as the point where the velocity gradient with depth is at its negative extremum. The *S*-velocity of this high-velocity lithosphere is not significantly higher than that of *iasp91* at moderate upper mantle depths. Assuming that these high *S*-velocities are caused predominantly by lower temperatures [Jordan, 1988] but also by a depleted composition, this implies that the lithospheric root of the southern São Francisco craton is not as cold or as depleted as the higher velocity cratonic root of the Amazonian craton. This is not unlikely given the narrow width of the craton and its proximity to the 120 Ma Paraná basin and oceanic mantle.

6.3. Mantle wedge between Andean crust and subducting Nazca plate

Upper mantle structure in western South America is dominated by more recent and presently on-going processes related to subduction of the Nazca plate beneath the South American plate. The geometry of the subducting Nazca plate is most prominently outlined by the seismicity of the Wadati-Benioff zone [Hasegawa and Sacks, 1981; Cahill and Isacks, 1992; Engdahl et al., 1997]. In several regions SA99 shows high velocity material along the inter- and extrapolated Wadati-Benioff zone beneath the Andes (Plate 3),

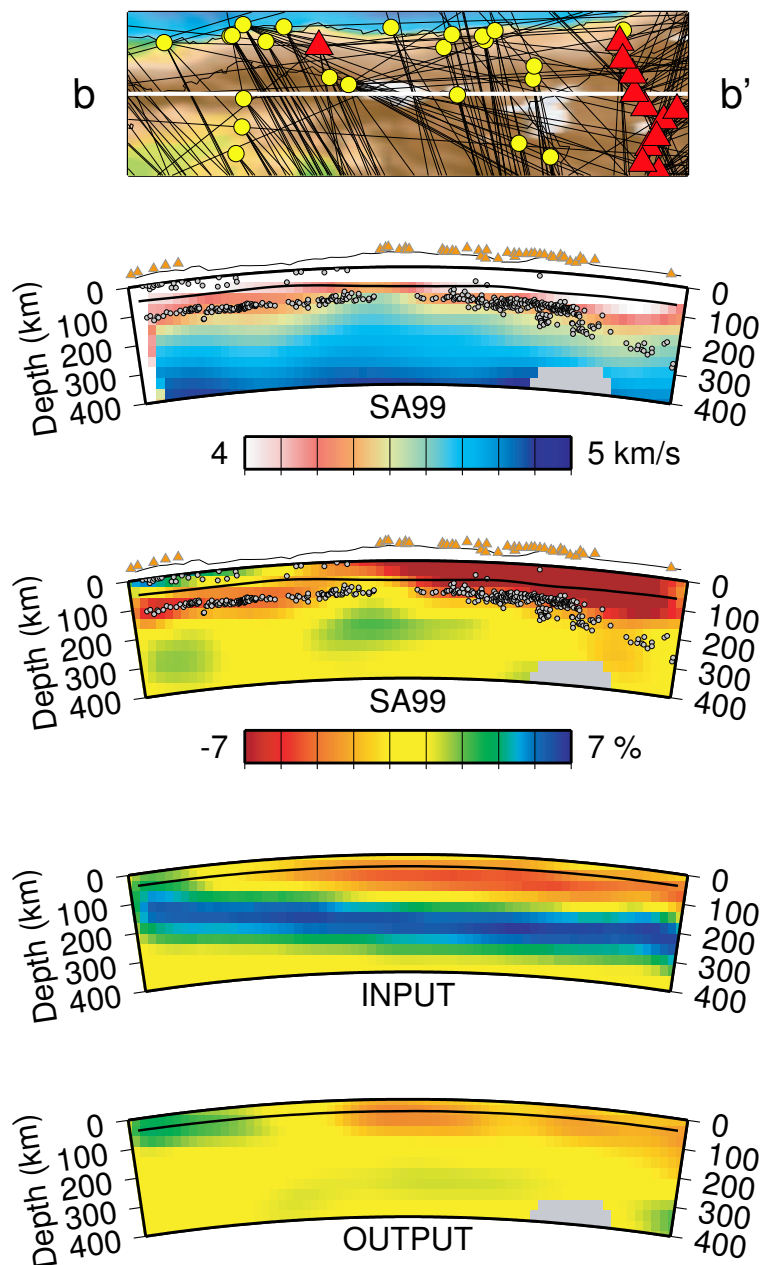


Plate 3b. Same as Plate 3a but for cross section bb'.

in agreement with the expected location of subducted Nazca lithosphere. These high velocities do not form a continuous unit due to variations in resolution for the subducting Nazca lithosphere (Plate 3). Although our data cannot resolve subducting lithosphere at a depth of 200 km for profile cc', the resolution is better around 300 km and it is likely that the high velocity anomaly in SA99 at 300 km just north-east of the Andes (Plate 3c) represents a deeper part of the subducting Nazca plate. This interpretation would allow a northward extension of the 300 km slab contour of Cahill and *Isacks* [1992] (Plate 2) and implies a near-vertical dip of the subducting plate below 200 km. This would be consistent with the cluster of deep earthquakes [Engdahl *et al.*, 1998] in this region and with results from *James and Snoke* [1990]. Teleseismic arrival time tomography shows more uniform resolving power below 100 km for the subducting Nazca plate [Engdahl *et al.*, 1995; VanDecar *et al.*,

1995b; *Bijwaard et al.*, 1998] than our predominantly continental body and surface waveform tomography.

In regions along the Andes that are volcanically active SA99 shows extremely low *S*-velocities in the continental mantle wedge directly above the Wadati-Benioff zone, which are well resolved (Plate 3). These regions correlate with the regions of historic and present volcanic activity (see map at 100 km in Plate 2). The depth extent of this low velocity anomaly of the mantle wedge increases with increasing dip of the Nazca slab, reaching its maximum around a depth of 150 km (Plate 2 and 3). This low velocity anomaly is located immediately adjacent to the Wadati-Benioff zone, which suggests that the origin of the anomaly is related to the subducting oceanic crust below it. Also, the clear boundary of the anomaly on the continental side shows no continuity with a possible sub-continental low *S*-velocity channel.

In general, a lowered *S*-velocity can be achieved by elevated temperature or anomalous composition, such as the presence of partial

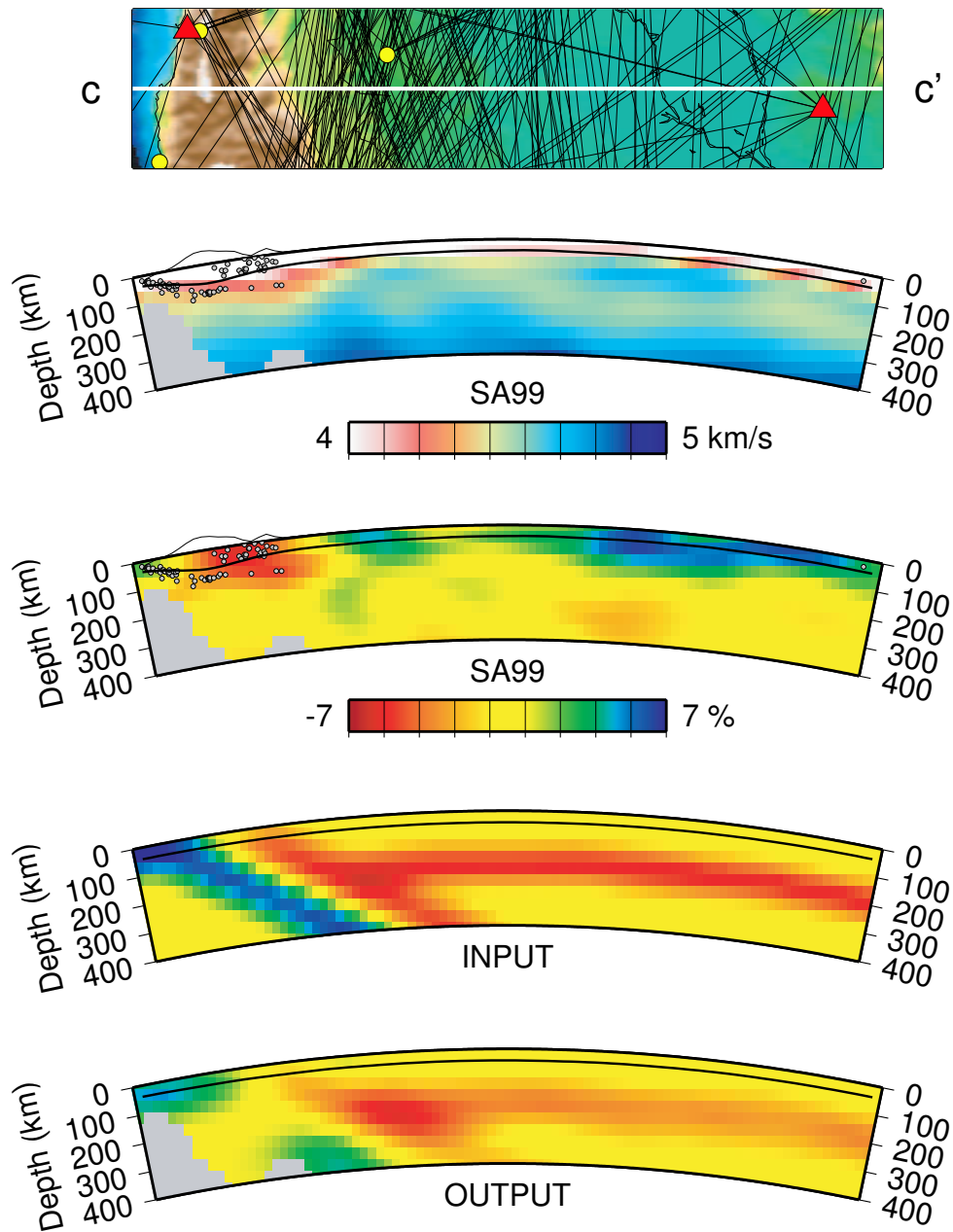


Plate 3c. Same as Plate 3a but for cross section cc'.

melt, volatiles, or a chemical enrichment in FeO. Chemical enrichment alone cannot explain the more than 10% lower velocities. In a dry mantle, anomalously high temperature in excess of 1500°C [Karato, 1993; Sobolev *et al.*, 1996; Goes *et al.*, 2000] would be required to explain such low velocities. It is difficult to identify a mechanism that creates and maintains such high temperatures in the direct vicinity of the subducting lithosphere, which is much colder than the adjacent mantle wedge. Only the mechanism of frictional heating of continental lithosphere under lateral compression [Kincaid and Silver, 1996] could create such high temperatures. However, it is unlikely that the low velocities in the mantle wedge are a pure thermal effect since Morris *et al.* [1990] have provided evidence that a typical mantle wedge is rich in volatiles like H_2O released by the subducting oceanic crust. Such volatiles would drastically lower the S -velocity in the mantle wedge, primarily by lowering the solidus. Even at normal upper mantle temperatures, the mantle wedge will be strongly fluxed by hydrous fluids and is

thus likely to contain partial melt. At an unelevated temperature of 1200°C a 2.5% peridotite melt fraction can exist in the mantle wedge at 0.15 wt% H_2O content [Gaetani and Grove, 1998; Ulmer, 2001] while only 1.1% fraction of melt or fluid in a realistic, organized cusped geometry is necessary to lower the S -velocity by 10% [Hammond and Humphreys, 2000]. This 10% is of the same magnitude as the lowered S -velocity in the mantle wedge of SA99. If the alkali-rich hydrous component in subducting Nazca crust is similar to that of the subducting crust at the Marianas, a melt/fluid fraction of as much as 4% can be present at only 1200°C [Gaetani and Grove, 1998]. This fraction would lower the S -velocity even more but can also be consistent with our 10% velocity reduction if the geometry of the melt or fluid is less organized [Hammond and Humphreys, 2000]. An unelevated temperature for the mantle wedge would be consistent with the Andean gravity and geoid profile if the crust is in isostatic equilibrium [Beck *et al.*, 1996; Froidevaux and Isacks, 1984].

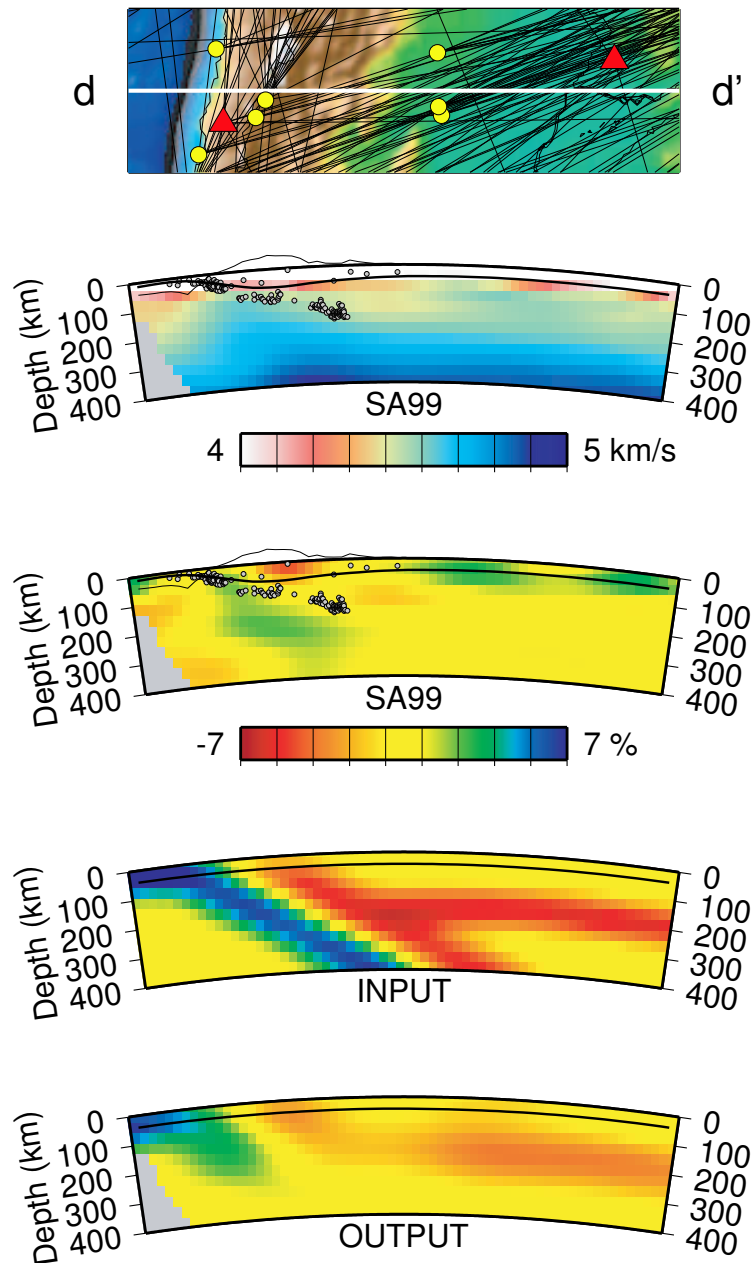


Plate 3d. Same as Plate 3a but for cross section dd'.

The low S -velocity mantle wedge of SA99 is not centered beneath the active western arc but extends across the entire Andes, including especially the eastern Altiplano and the eastern ranges (Plates 2 (100 km) and 3a,c). This observation lends some support to the argument that the low S -velocities are caused by hydration of the mantle through the release of volatiles from past periods of flat subduction, *e.g.* at 30 Ma in the central sector of the Andes [James and Sacks, 1999]. James and Sacks [1999] also explain the temporal shifts in types and locations of Andean volcanism as depending on slab dip and resultant degrees of hydration as well as cooling and reheating of the overlying continental mantle.

6.4. Mantle flow

Classical geochemical models for a mantle wedge [*e.g.* Hochstaedter *et al.*, 2000] require a continuous influx of enriched mantle material into the mantle wedge. Such an influx of enriched

mantle material has been included in numerical subduction models in the form of corner flow [Andrews and Sleep, 1974; Davies and Stevenson, 1992]. The origin of material flowing into the South American mantle wedge is unknown and could comprise the entire subcontinental upper mantle. The more material flows from continental upper mantle into the mantle wedge, the more the correlation between upper mantle structure and surface geology and tectonics would be disturbed. This disturbance could be evident in tomographic images of upper mantle structure, such as SA99, depending on the degree of disturbance. In order to use SA99 for investigating the origin of material fluxing into the South American mantle wedge we first estimate the rate of corner flow from Andean arc volcanism.

The volume of extrusive volcanism in the Andes has been estimated by Francis and Rundle [1986] to be 3 to 4 $\text{km}^3/\text{m.y.}$ per km arc length. Assuming a range of 0 to 80 $\text{km}^3/\text{m.y.}$ of corresponding intrusive volcanism and a range of 2.5% to 20% peridotite melt fraction (R. Carlson, personal communication, 2000) provides

minimum and maximum estimates of 15 and 3360 $km^3/m.y.$, respectively, for the influx of enriched mantle material into the mantle wedge. If this mantle material flows along an adiabat into the mantle wedge from a diffuse region of adjacent continental upper mantle, this influx would imply a material displacement range of 1 km to 250 km across a 400 km^2 interface within the mantle in the past 30 m.y.. These displacement estimates decrease when the interface across which the enriched mantle material fluxes into the mantle wedge is assumed wider, as is more likely further away from the wedge in the case of diffuse influx, and they would increase when this interface is assumed to be narrower, e.g. in the case of influx through a narrow low-viscosity channel. Channeled influx is not supported by SA99 since a low-viscosity channel would most probably be imaged as a low S -velocity anomaly connecting to the mantle wedge. Diffuse influx, however, would not be detectable in our seismic results as even the maximum estimate of around 250 km of displaced upper mantle material would not be identifiable in SA99 unless we knew the structure of the upper mantle at 30 Ma. Therefore we argue that SA99 excludes the possibility of channeled influx of low-viscosity material into the mantle wedge but is not inconsistent with the geochemically required corner flow, if it is in the form of diffuse influx of enriched mantle material.

7. Conclusions

Continental-scale, broad-band seismograms combined from portable and permanent South American seismic networks provide excellent wave path coverage for the central and western part of the continent. We used the S - and surface wave forms from mainly the global, BLSP and BANJO networks to derive 3-D upper mantle S -velocity model SA99. Model SA99 is well resolved in depth owing to the combination of fundamental and higher mode surface waves in our inversion. The lateral resolution of SA99 is heterogeneous, and is best in central and western South America, owing to wave path coverage that is dense and well distributed over azimuth. Trade-offs between upper mantle S -velocity and depth to the Moho have been largely eliminated by incorporating additional constraints on crustal thickness from receiver function analysis and by assuming Airy isostatic equilibrium. High resolution images are thus obtained for continental upper mantle structure beneath the Andes as well as beneath significant parts of the South American platform.

In general, SA99 shows that the large-scale tectonic and geologic domains of South America are reflected in corresponding upper mantle heterogeneity, showing variations in S -velocity of up to 1 km/s above 100 km. Our seismic modeling also precludes the possibility that South American plate motion is decoupled from upper mantle motion along a laterally uniform low-viscosity layer.

In particular, resolved parts of the upper mantle structure beneath the western Guyana and Guaporé shields are shown to represent high-velocity lithosphere. This indicates that both shields are underlain by cratonic lithosphere of the Precambrian Amazonian craton. Despite Mesozoic rifting, the Amazon basin between the two shields is also underlain by high-velocity lithosphere, extending as least as deep as that of the surrounding shields. Moreover, this post-Precambrian rifting does not seem to have affected the continuity of the high-velocity lithosphere of the Amazonian craton within the resolution of our data.

In contrast to the Amazon basin, other intra-platform basins of central and western South America are typically underlain by low velocity upper mantle. The low velocities beneath the Pantanal and Chaco basins extend from beneath the crust to, locally, depths of 350 km. Most probably the upper mantle beneath these basins is several hundreds of degrees warmer than normal mantle material. The uppermost mantle under the Paraná basin shows slightly low velocities in the west and higher velocities in the east. At larger depths under

the eastern Paraná basin a strong low velocity anomaly confirms results from teleseismic arrival time tomography postulating a fossil plume here.

Along the volcanically active parts of the Andes we find a well resolved mantle wedge with extremely low S -velocities below an extremely thick crust. The bottom of the low velocity mantle wedge is immediately adjacent to the Wadati-Benioff zone and thus to the subducting oceanic crust. The most consistent explanation of these low velocities in the mantle wedge is 2.5% to 4% partial melt in a realistic geometry, which is generated at temperatures near 1200°C in reaction to realistic amounts (0.15 wt%) of volatiles released from the subducting oceanic crust. Geochemical and petrological observations require active corner flow to refresh the mantle wedge with enriched mantle material. SA99 permits diffuse influx of material from the continental upper mantle into the mantle wedge but is not consistent with influx through a low-viscosity channel.

Acknowledgments. We greatly acknowledge the accomplishments of Randy Kuehnel in running many of the temporary networks used in this analysis. We particularly thank Marcelo Assumpção, Rick Carlson, and Tim Grove for discussions on South American geology and geophysics, geochemistry, and petrology, respectively. The clarity and focus of the original manuscript were greatly improved thanks to constructive review comments provided by Guust Nolet and Steve Grand. The work presented here was supported by the Carnegie Institution of Washington (CIW) and NSF-US grants EAR-9304503 and EAR-9304560. Data were recorded through the efforts of field crew from the Department of Terrestrial Magnetism (DTM) of the CIW, the University of Arizona, the Instituto Astronômico e Geofísico of São Paulo, Brazil, the San Calixto Observatory, Bolivia, and the Global Seismic Network, and were made available through DTM and the IRIS Data Management Center (<http://www.iris.edu>). The Eidgenössische Technische Hochschule in Zürich, Switzerland, and the DTM provided support during the writing of this paper. Plates and figures were produced with the Generic Mapping Tools.

References

- Andrews, D.J., and N.H. Sleep, Numerical modelling of tectonic flow behind island arcs, *Geophys. J. R. astr. Soc.*, **38**, 237–251, 1974.
- Assumpção, M., D. James and A. Snoko, Crustal thicknesses in SE Brazilian shield by receiver function analysis: Implications for isostatic compensation, *J. Geophys. Res.*, **107**, 10.1029/2001JB000422, 2002.
- Beck, S., P.G. Silver, G. Zandt, T. Wallace, S. Myers, R. Kuehnel, S. Ruppert, L. Drake, E. Minaya, P. Soler, P. Baby, S. Barrientos, J. Telleria, M. Tinker and J. Swenson, Across the Andes and along the Altiplano: a passive seismic experiment, *IRIS Newsletter*, **8**, 1–2, 1994.
- Beck, S.L., G. Zandt, S.C. Myers, T.C. Wallace, P.G. Silver and L. Drake, Crustal-thickness variations in the central Andes, *Geology*, **24**, 407–410, 1996.
- Bijwaard, H., W. Spakman and E.R. Engdahl, Closing the gap between regional and global travel time tomography, *J. Geophys. Res.*, **103**, 30,055–30,078, 1998.
- Cahill, T. and B.L. Isacks, Seismicity and shape of the subducted Nazca plate, *J. Geophys. Res.*, **97**, 17503–17529, 1992.
- Cordani, U.G. and B.B. de Brito Neves, The geologic evolution of South America during the Archaean and early Proterozoic, *Rev. Bras. de Geoc.*, **12**, 87–88, 1982.
- Davies, J.H. and D.J. Stevenson, Physical model of source region of subduction zone volcanics, *J. Geophys. Res.*, **97**, 2037–2070, 1992.
- Das, T. and G. Nolet, Crustal thickness estimation using high frequency Rayleigh waves, *Geophys. Res. Lett.*, **22**, 539–542, 1995.
- Dost, B., A. van Wettum, and G. Nolet, The NARS Array, *Geol. Mijnbouw*, **63**, 318–386, 1984.
- Dziewonski, A.M., A.L. Hales, and E.R. Lapwood, Parametrically simple Earth models consistent with geophysical data, *Phys. Earth Planet. Inter.*, **10**, 12–48, 1975.
- Engdahl, E.R., R.D. van der Hilst and J. Berrocal, Imaging of subducted lithosphere beneath South America, *Geophys. Res. Lett.*, **22**, 2317–2320, 1995.

- Engdahl, E.R., R.D. van der Hilst, S.H. Kirby, S. Widiyantoro, A survey of South American slab structures and internal processes using a new combined data base of high-resolution earthquake hypocenters, tomographic images and focal mechanism data, *Eos Trans. A.G.U.*, 78, 446–446, 1997.
- Engdahl, E.R., R. van der Hilst and R. Buland, Global teleseismic earthquake relocation with improved travel times and procedures for depth determination, *Bull. Seism. Soc. Am.*, 88, 722–743, 1998.
- Ekström, G. and A. Dziewonski, The unique anisotropy of the Pacific upper mantle, *Nature*, 394, 168–172, 1998.
- Francis, P.W. and C. Rundle, Rates of production of the main magma types in the central Andes, *Bull. Geol. Soc. Am.*, 87, 474–480, 1986.
- Froidevaux, C. and B.L. Isacks, The mechanical state of the lithosphere in the Altiplano-Puna segment of the Andes, *Earth Planet. Sci. Lett.*, 71, 305–314, 1984.
- Gaetani, G.A. and T.L. Grove, The influence of water on melting of mantle peridotite, *Contrib. Min. Petrol.*, 131, 323–346, 1998.
- Gansser, A., Facts and theories about the Andes, *J. Geol. Soc.*, 129, 93–131, 1973.
- Gibbs, A.K. and K.R. Wirth, Origin and evolution of the Amazonian craton. In: *Early crustal genesis: The world's oldest rocks, LPI Technical Report*, 46–50, 1986.
- Goes, S., R. Govers and P. Vacher, Shallow mantle temperatures under Europe from P and S wave tomography, *J. Geophys. Res.*, 105, 11,153–11,169, 2000.
- Gomberg, J.S., K.F. Priestly, T.G. Masters and J.N. Brune, The structure of the crust and upper mantle of northern Mexico, *Geophys. J. R.A.S.*, 94, 1–20, 1988.
- Grand, S.P., Mantle shear structure beneath the Americas and surrounding oceans, *J. Geophys. Res.*, 99, 11,591–11,621, 1994.
- Hammond, W.C. and E.D. Humphreys, Upper mantle seismic wave velocity: Effects of realistic partial melt geometries, *J. Geophys. Res.*, 105, 10975–10986, 2000.
- Hasegawa, A. and I.S. Sacks, Subduction of the Nazca plate beneath Peru as determined from seismic observations, *J. Geophys. Res.*, 86, 4971–4980, 1981.
- Hochstaedter, A.G., J.B. Gill, B. Taylor, O. Ishizuka, M. Yuasa and S. Morita, Across-arc geochemical trends in the Izu-Bonin arc: Constraints on source composition and mantle melting, *J. Geophys. Res.*, 105, 495–512, 2000.
- Horton, B.K. and P.G. DeCelles, The modern foreland basin system adjacent to the central Andes, *Geology*, 25, 895–898, 1997.
- James, D.E., Andean crustal and upper mantle structure, *J. Geophys. Res.*, 76, 3246–3271, 1971a.
- James, D.E., Plate tectonic model for the evolution of the Central Andes, *Geol. Soc. Am. Bull.*, 82, 3325–3346, 1971b.
- James, D.E., M. Assumpção, J.A. Snoke, L.C. Ribotta and R. Kuehnel, Seismic studies of continental lithosphere beneath SE Brazil, *An. Acad. bras. Ci.*, 65, 227–250, 1993.
- James, D.E. and J.A. Snoke, Seismic evidence for continuity of the deep slab beneath central and eastern Peru, *J. Geophys. Res.*, 95, 4989–5001, 1990.
- James, D.E. and I.S. Sacks, Cenozoic formation of the central Andes: A geophysical perspective, *Spec. Pub. 7 of the SEG*, 1–25, 1999.
- Jordan, T.H., Structure and formation of the continental tectosphere, *J. Petrol., Special Lithosphere Issue*, 11–37, 1988.
- Karato, S., Importance of anelasticity in the interpretation of seismic tomography, *Geophys. Res. Lett.*, 20, 1623–1626, 1993.
- Kennett, B.L.N. and E.R. Engdahl, Travel times for global earthquake location and phase identification, *Geophys. J. Int.*, 105, 429–465, 1991.
- Kennett, B.L.N. and S. Widiyantoro, A low seismic wavespeed anomaly beneath northwestern India: a seismic signature of the Deccan Plume?, *Earth Planet. Sci. Lett.*, 165, 145–155, 1999.
- Kincaid, C. and P. Silver, The role of viscous dissipation in the orogenic process, *Earth Planet. Sci. Lett.*, 142, 271–288, 1996.
- Lebedev, S. and G. Nolet, The upper mantle beneath SE Asia, I: S-velocity tomography, submitted to *J. Geophys. Res.*, 2001.
- Li, X., and B. Romanowicz, Global mantle shear velocity model developed using nonlinear asymptotic coupling theory, *J. Geophys. Res.*, 101, 22245–22272, 1996.
- Meijer, P.Th. and M.J.R. Wortel, The Dynamics of Motion of the South American Plate, *J. Geophys. Res.*, 97, 11915–11931, 1992.
- Milani, E.J. and P.V. Zalán, An outline of the geology and petroleum systems of the Paleozoic interior basins of South America, *Episodes*, 22, 199–205, 1999.
- Morris, J.D., W.P. Leeman and F. Tera, The subducted component in island arc lavas: constraints from Be isotopes and B-Be systematics, *Nature*, 344, 31–36, 1990.
- Mooney, W.D., G. Laske and T.G. Masters, CRUST 5.1: A global crustal model at 5° × 5°, *J. Geophys. Res.*, 103, 727–747, 1998.
- Myers, S.C., S. Beck, G. Zandt and T. Wallace, Lithospheric-scale structure across the Bolivian Andes from tomographic images of velocity and attenuation for P and S waves, *J. Geophys. Res.*, 103, 21233–21252, 1998.
- Nishimura, C.E. and W.F. Forsyth, The anisotropic structure of the upper mantle in the Pacific, *Geophys. J.*, 96, 203–229, 1989.
- Nolet, G., Partitioned Waveform Inversion and Two-Dimensional Structure Under the Network of Autonomously Recording Seismographs, *J. Geophys. Res.*, 95, 8499–8512, 1990.
- Piccirillo, E.M. and A.J. Melfi (eds), The Mesozoic flood volcanism of the Paraná Basin, Instituto Astronômico e Geofísico Publishers, São Paulo, 600 pp., 1988.
- Ramos, V.A., Plate tectonic setting of the Andean Cordillera, *Episodes*, 22, 183–190, 1999.
- Richardson, W.P., E.A. Okal, and S. van der Lee, Rayleigh-wave tomography of the Ontong-Java Plateau, *Physics of the Earth and Planetary Interiors*, 118, 29–51, 2000.
- Russo, R.M., P.G. Silver, M. Franke, W.B. Ambeh, D.E. James, Shear-wave splitting in Northeast Venezuela, Trinidad, and the eastern Caribbean, *Phys. Earth Planet. Inter.*, 95, 251–275, 1996.
- Russo, R. and P.G. Silver, Cordillera formation, mantle dynamics, and the Wilson Cycle, *Geology*, 24, 511–514, 1996.
- Silver, P.G., R.M. Russo and C. Lithgow-Bertelloni, The coupling of plate motion and plate deformation, *Science*, 279, 60–63, 1998.
- Sacks, I.S. and H. Okada, A comparison of the anelasticity structure beneath western South America and Japan, *Phys. Earth Planet. Inter.*, 9, 211–219, 1974.
- Sambridge, M. and O. Gudmundsson, Tomographic systems of equations with irregular cells, *J. Geophys. Res.*, 103, 773–781, 1998.
- Satzmari, P., Amazon Rift and Picso-Jurua Fault; their relation to the separation of North America from Gondwana, *Geology*, 11, 300–304, 1983.
- Schimmel, M., M. Assumpção and J.C. VanDecar, Seismic Velocity Anomalies Beneath SE Brazil From P- and S-Wave Travel Time Inversions, *J. Geophys. Res.*, in press, 2001.
- Simons, F.J., A. Zielhuis, and R.D. van der Hilst, The deep structure of the Australian continent from surface wave tomography, *Lithos*, 48, 17–43, 1999.
- Snoke, J.A. and D.E. James, Lithospheric structure of the Chaco and Paraná basins of South America from surface-wave inversion, *J. Geophys. Res.*, 102, 2939–2951, 1997.
- Sobolev, S.V., H. Zeyen, G. Stoll, F. Werling, R. Altherr and K. Fuchs, Upper mantle temperatures from teleseismic tomography of French Massif Central including effects of composition, mineral reactions, anharmonicity, anelasticity and partial melt, *Earth Planet. Sci. Lett.*, 139, 147–163, 1996.
- Tassinari, C.C.G. and M.J.B. Macambira, Geochronological provinces of the Amazonian craton, *Episodes*, 22, 174–182, 1999.
- Ulmer, P., Partial melting in the mantle wedge – The role of H₂O in the genesis of mantle-derive “arc-related” magmas, *Phys. Earth Planet. Inter.*, in press, 2001.
- Ussami, N., S. Shiraiwa and J.M. Landim Dominguez, Basement reactivation in a sub-Andean foreland flexural bulge: The Pantanal wetland, SW Brazil, *Tectonics*, 18, 25–39, 1999.
- VanDecar, J.C., D.E. James and M. Assumpção, Seismic evidence for a fossil mantle plume beneath South America and implications for plate driving forces, *Nature*, 378, 25–31, 1995a.
- VanDecar, J.C., D. James, P. Silver, M. Assumpção, S. Myers, S. Beck, T. Wallace, G. Zandt, E. Minaya, G. Asch, R. Kuehnel, Mantle structure beneath central South America, *Eos Suppl.*, 76, F606–F606, 1995b.
- Van der Lee, S., The earth's upper mantle: its structure beneath North America and the 660-km discontinuity beneath northern Europe, *Ph.D. thesis, Princeton University*, 186 pp., 1996.
- Van der Lee S. and G. Nolet, Upper mantle S-velocity structure of North America, *J. Geophys. Res.*, 102, 22815–22838, 1997.
- Van der Lee, S., Observations and origin of Rayleigh-wave amplitude anomalies, *Geophys. J. Int.*, 135, 691–699, 1998.
- Van der Lee, S., D. James, and P. Silver, Continental upper mantle structure from combined data from mobile broadband networks in South America, *ORFEUS Newsletter*, 2, 14, 2000.
- Vdovin, O., J.A. Rial, A.L. Levshin and M.H. Ritzwoller, Group velocity tomography of South America and the surrounding oceans, *Geophys. J. Int.*, 136, 324–340, 1999.
- Zielhuis, A. and G. Nolet, Shear-wave velocity variations in the upper mantle beneath central Europe, *Geophys. J. Int.*, 117, 695–715, 1994.

Suzan van der Lee (corresponding author), ETH-Hönggerberg (HPP),
CH-8093 Zürich, Switzerland (suzan@tomo.ig.erdw.ethz.ch)

David James and Paul Silver, Department of Terrestrial Magnetism,
Carnegie Institution of Washington, 5241 Broad Branch Rd. NW, Wash-

ington DC 20015, USA (james@dtm.ciw.edu; silver@dtm.ciw.edu)

(Received June 1, 2000; revised December 8, 2000;
accepted March 8, 2001.)